

## Precision Measurement of the Cosmic Ray Boron-to-Carbon Ratio with AMS

A. OLIVA<sup>1</sup> ON BEHALF OF THE AMS COLLABORATION<sup>2</sup>.

<sup>1</sup> *Centro de Investigaciones Energéticas, Medioambientales y Tecnológicas, CIEMAT, E-28040 Madrid, Spain.*

<sup>2</sup> *for the complete list of authors see the AMS Collaboration list in these proceedings.*

*alberto.oliva@cern.ch*

**Abstract:** AMS-02 is wide acceptance high-energy physics experiment operating since May 2011 onboard of the International Space Station. AMS precisely distinguishes the nuclear component of the cosmic rays (CRs) from charge  $Z = 1$  up to at least  $Z = 26$  in a kinetic energy range from GeV/n to TeV/n. Among the CRs nuclei measurements the Boron-to-Carbon fluxes ratio is one of the most sensitive observables for the propagation modeling, being a Boron a secondary product of spallation of heavier primary elements present in cosmic rays such as Carbon and Oxygen. AMS-02 detector separates Carbon from Boron with a contamination of less than  $10^{-4}$ , using the charge measurement delivered by the Silicon Tracker and by the Time-of-Flight. Effect of inelastic interactions in AMS materials, such as flux attenuation or charge-changing interactions (as  $C \rightarrow B$ ) are controlled by the comparison of charge measured by detector located inside AMS with those located on the top of the instrument. A determination of the B/C ratio measured by AMS is presented in the kinetic energy interval from 0.5 to 670 GeV/n.

**Keywords:** Cosmic Rays Nuclei, B/C ratio, AMS Experiment.

### 1 AMS Experiment

The layout of the AMS-02 detector [1] is shown in fig. 1. It consists of nine planes of precision Silicon Tracker, a transition radiation detector (TRD), four planes of time of flight counters (TOF), a permanent magnet, an array of anti-coincidence counters (ACC), surrounding the inner tracker, a ring imaging Čerenkov detector (RICH), and an electromagnetic calorimeter (ECAL).

Silicon Tracker measures the particle rigidity ( $R = p/Z$ ), its charge sign and evaluates the absolute charge magnitude ( $Z$ ). Rigidity and sign are derived from the measurement of the curvature of the particle in the 1.4 kG AMS magnetic field. Particle trajectory is determined by the coordinate measurement along the 9 layers (L1, ..., L9) of 300  $\mu\text{m}$  thick double-side micro-strip Silicon sensors. With a spatial resolution of about 7  $\mu\text{m}$  ( $2 \leq Z \leq 6$ ) and a maximum lever arm of about 3 m, the maximum detectable rigidity (MDR), i.e.  $R$  corresponding to  $\Delta R/R = 100\%$ , is estimated to be around 3 TV [2] [3]. Each Tracker layer delivers an estimation of the particle charge magnitude from the energy deposition measurement ( $\propto Z^2$ ) in a wide charge range  $1 \leq Z \leq 26$ . The 7 independent measurement of charge in the Inner Tracker (from L2 to L8) can be combined together achieving a charge resolution of 0.12 charge units (c. u.) for Carbon [4].

TOF system is composed by four planes of 1 cm thick polyvinyl-toluene counters two located above (Upper TOF or UTOF) and two below the magnet (Lower TOF or LTOF). TOF provides the charged particle trigger of the experiment, delivering a measurement of the velocity and discriminating between upward- and downward-going particles. Velocity resolution for  $\beta = 1$ ,  $Z = 1$  particles is  $\Delta\beta = 0.04$ , and improves with increasing magnitude of charge to a limit of  $\Delta\beta = 0.01$  for  $Z > 5$  particles. The 4 independent charge determination coming from the energy deposition measurement on each of the 4 TOF layers have a very wide range (up to  $Z = 40$ ) and a charge resolution of about 0.16 c.u. for Carbon [5].

The ACC veto system is composed by scintillating paddles arranged in a cylindrical shape surrounding the Inner Tracker. Its main purpose is to reject the large amount of horizontal events interacting in the magnet structure.

The RICH is designed to measure the velocity and the magnitude of the charge of cosmic rays from the Čerenkov radiation emitted by particles passing through the radiator plane located below the LTOF. The estimated velocity resolution for  $\beta = 1$ ,  $Z = 1$  particles is  $\Delta\beta = 10^{-3}$ , improving with charge up to a limit of  $\Delta\beta = 5 \cdot 10^{-4}$  with a resolution in charge of 0.32 c.u. for Carbon [6].

TRD and ECAL are specialized detectors designed to reach a high capabilities in electron/proton separation[10]. They are located at the two edges of AMS. These two detectors have also good capabilities in the measurements of charge [7] [8] and are used in the ion analysis to construct control samples.

### 2 Data Analysis

Data collected in the first 2 years of AMS operation have been analyzed. Reconstruction algorithms able to associate information of the various sub-detectors were optimized for the search of  $Z > 1$  particles, trying to avoid the abundant physical noise background given by  $\delta$ -rays production. Accurate time dependent calibrations account for the space environmental conditions rapid changes [2] [4] [5] [6] [7] [8].

MonteCarlo (MC) simulated events are produced using GEANT4-4.9.4 package [12]. The simulation includes an accurate description of AMS-02 materials and geometry, specific digitization algorithms able to reproduce the detector responses, and physics models of electromagnetic and hadronic interaction. For a better understanding of the nuclei interaction inside the detector two kind of hadronic simulation were adopted, the default GEANT4 physics list [12], and the DPMJET-II.5 [13] as an alternative model for energies above 5 GeV/n.

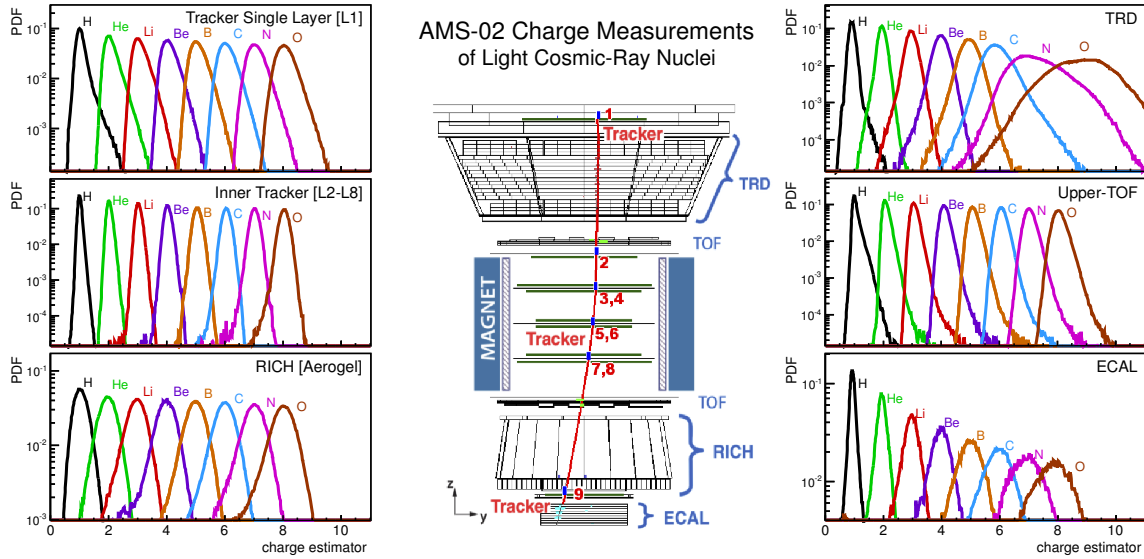


**Fig. 1:** An event traversing AMS detector [9]. Particle charge magnitude is evaluated several times along the particle trajectory: (a) on top of AMS by a layer of Silicon sensors constituting the Upper Tracker (L1); (b) in the TRD by the combination of measurements in the 20 layers of straw tubes; (c) in the Inner Tracker by the combination of 7 single layer Tracker measurements (from L2 to L8); (d) in the Upper TOF (UTOF) by the combination of the measurements of two layers of scintillating counters; on the Lower TOF (LTOF) similarly to UTOF; (e) in the RICH by counting the number of photons emitted by the Čerenkov emission; on the Lower Tracker (L9); and (f) by the the energy deposit measurement in the first layers of ECAL.

Particle fluxes are suppressed by the geomagnetic cutoff. To take into account the effect of the cutoff only particles with rigidity greater than  $1.5 \cdot R_C$  are used in this analysis, where  $R_C$  is the maximum rigidity cutoff in the AMS field of view obtained from the Størmer estimation [14] given the AMS geomagnetic coordinates and zenith direction. Periods of not nominal detector acquisition were also discarded in the analysis.

Finally in the  $Z > 2$  nuclear component is pre-selected using cuts on Tracker Inner charge ( $Q_{IT} > 2.5$ ) and on the Tracker L1 charge ( $Q_{L1} > 2.5$ ). This pre-selected sample accounts of about 23M particles with  $Z > 2$ .

### 3 Ratio Measurement

Boron-to-Carbon relative abundance is defined as the ratio of the two species fluxes. The differential energy spectrum of the particles in the kinetic energy bin  $[K_n, K_n + \Delta K]$  is related to the observed number of counts  $N(K_n, K_n + \Delta K)$  by:

$$\Phi(\bar{K}_n) = \frac{N(K_n, K_n + \Delta K)}{A \cdot \varepsilon \cdot \Delta T \cdot \Delta K}$$

where  $A$  is the geometrical acceptance ( $\text{m}^2\text{sr}$ ) determined with MC. Acceptance is modified by  $\varepsilon$ , the combination of estimated efficiencies (selection, purity, trigger, track efficiency, survival probability). While  $\Delta T = \Delta T(R)$  is the exposure time, i.e. the amount of seconds corrected for data acquisition lifetime in orbits with  $R > 1.5 \cdot R_C$ .

#### 3.1 Number of Counts

Boron and Carbon samples are easily separated using the TOF and Inner Tracker by means of simple cuts on the charge estimators. Efficiency of the selection is very high,

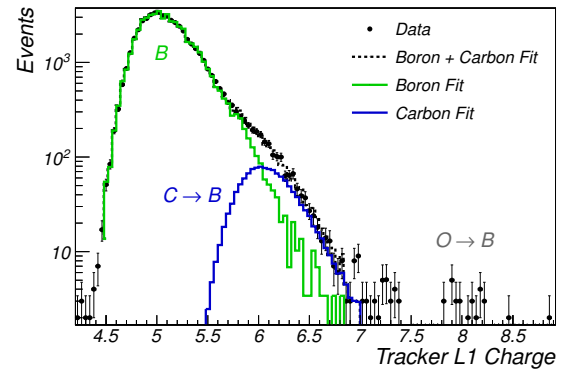


**Fig. 2:** Charge distribution of L1 for a selection of Boron with TOF and Inner Tracker. Primary Carbon and Oxygen interacting in materials below L1 can be estimated by a reference spectrum fit.

up to 98%. Probability of assigning to a particle of charge  $Z$  a wrong charge is less than  $10^{-4}$ .

#### 3.2 Purity Estimation

Nuclei may interact on AMS materials and split into fragments of lower charge. This events can be recognized by a higher charge measured on top of AMS and a lower charge measured with detector located below. The fig. 2, filled circles, presents the charge distribution on top of AMS measured by L1 for a selection of Boron with TOF and Inner Tracker. The population of Oxygens and Carbons corresponds to the charge-changing processes  $O \rightarrow B$  and  $C \rightarrow B$  happening between L1 and UTOF.

Criteria based on properties of the fragmentation process,

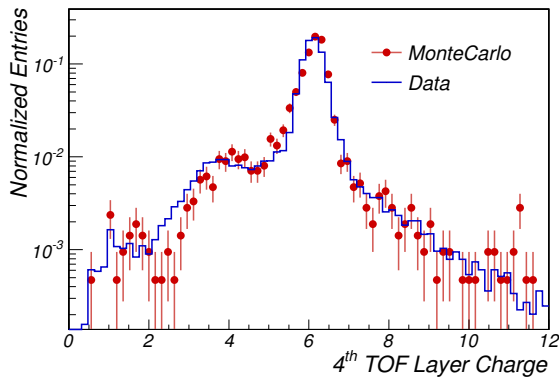


**Fig. 3:** Charge distribution of TOF Layer 4 for a selection of incoming Carbon on L1. The good agreement between data and MC in the peak region, and in the interaction generated tail, indicate a good modeling of hadronic interactions and materials description between L1 and LTOF.

as the presence of more than one track with high momentum, were developed to reduce this background. The selection efficiency for the criteria applied has been determined with an iterative procedure validated with MC samples for which the true selection efficiency is known. This efficiency has been evaluated being more than 70% for both Boron and Carbon. The ratio of Boron and Carbon selection efficiencies is flat and around 1 for rigidities  $R > 2$  GV.

To estimate the purity of the sample on L1 a fitting procedure has been developed. Reference spectra for each charge were derived and used to fit the distribution obtained after cuts, as presented in fig. 2. Purity of the sample is  $> 95\%$  for Boron and  $> 99.9\%$  for Carbon and is estimated with an accuracy of 0.1% on all the energy range.

### 3.3 Fragmentation Estimation

Acceptance is influenced by the probability that the nucleus does not undergo a fragmentation process along the AMS volume. This survival probability is calculated using a MC simulation of nuclear inelastic interaction on AMS materials. The interaction simulation has been validated with data making a comparison of specific interaction channels.

In fig. 3 is presented the charge measured on the fourth TOF layer (down-stream detector) for a selection of Carbon on the L1 and UTOF (up-stream detector). The agreement of the distributions indicates that fragment production is similar in data and MC.

A more quantitative approach uses charge selection on L1 and in the Inner Tracker to look for specific fragmentation channels. Boron and Carbon fragmentation into lighter elements as Boron, Beryllium and Lithium were compared between data and MC. Fragmentation fraction have typical value of 5%. Energy dependence has been also investigated using a similar approach of section 3.5. Data and Monte-Carlo show an agreement at 2% level.

### 3.4 Trigger Efficiency

Production of  $\delta$ -rays for nuclei is quite abundant. Emitted  $\delta$ -rays can fire counters of the veto system. To avoid consequent veto on nuclear events a specific trigger has been implemented in the level-one trigger logic. When a  $Z > 1$  particle traverses the TOF a trigger signal named *Big-Z* is

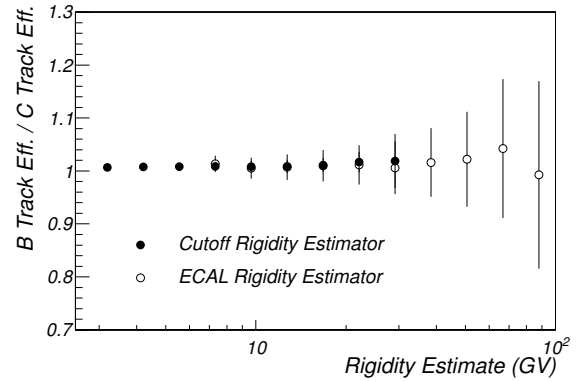


**Fig. 4:** The ratio between Boron and Carbon track efficiency is shown. Rigidity cutoff and the ECAL energy deposition are used to evaluate the track efficiency dependence with energy. A 2% difference of tracking efficiency flat with energy has been measured.

emitted and the condition on the veto counters is released ( $n. ACC < 5$ ). Moreover if the nucleus is passing through the ECAL the veto condition is completely removed. This second kind of trigger avoids event suppression because of backscplash from calorimeter.

A sample of events with a loose trigger condition (3 layer of TOF fired, no condition on ACC) is used to study the trigger efficiency. This unbiased sample is acquired with pre-scaling factor of 1/100 in order to have a reasonable acquisition rate. Boron and Carbon trigger efficiency is over 95%, while the differences between the two is less than 1%.

### 3.5 Track Efficiency

Track efficiency is the probability of reconstructing a track for an event passing through the Tracker.

A sample of events with a TOF standalone reconstruction is used to study the track efficiency. TOF is able to reconstruct by itself the particle direction, velocity and charge. This reconstruction can be strengthened using the TRD, that delivers a more precise track direction, and using the highest charge hit on L1, to clean-up from charge changing processes. Tracking efficiency is defined as the fraction of times a track with good properties is found in this sample.

The study of the track efficiency as function of energy is done using two estimators: (a) the Størmer cutoff expected from the particle incoming direction and (b) the energy deposition on ECAL. In fig. 4 the tracking efficiency ratio between Boron and Carbon is shown. A difference of about 2% approximately flat up to 100 GV been measured. MC shows a similar behavior.

### 3.6 Isotopic Composition

Tracker measures the particle rigidity. The rigidity to kinetic energy conversion required the  $A/Z$  ratio of each charged species.

$$K_n = \sqrt{\left(\frac{Z}{A} \cdot R\right)^2 + \left(\frac{M}{A}\right)^2} - \frac{M}{A}$$

Single fluxes in rigidity are firstly calculated, then converted into kinetic energy following different  $A/Z$  hypothesis for the different isotopes. Then spectra are summed using as weight the isotopic composition. Carbon has been as-

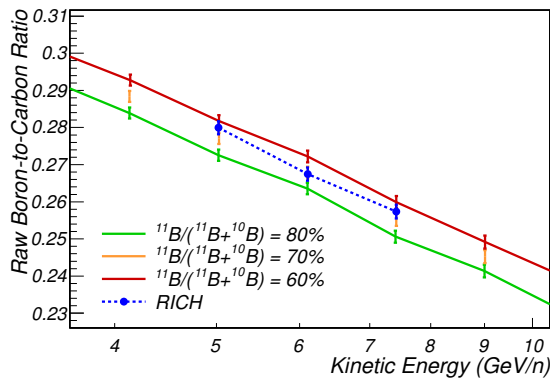


**Fig. 5:** Boron-to-Carbon ratios measured by Tracker derived using different Boron isotope mixtures hypothesis. The RICH measurement of the Boron-to-Carbon ratio is superimposed. With the orange line is indicated the chosen Boron isotopic mixture. The area between the red and the green line is accounted as systematic error.

sumed to be purely composed by  $^{12}\text{C}$  and Boron to have a relative abundance of  $^{11}\text{B}/(^{10}\text{B} + ^{11}\text{B}) = 0.7$ . This assumption has been cross-checked with the direct measurement of velocity, hence kinetic energy per nucleon, measured by RICH for energies between 5 and 8 GeV/n. In fig. 5 is presented the raw ratio determined with Tracker under several isotopic mixture hypothesis and the RICH direct measurement. RICH determination favors values around 0.7 for the isotopic mixture. A 10% error on Boron composition has been considered as systematic error. This translates into a  $\sim 1\%$  systematic error on the Boron-to-Carbon ratio.

### 3.7 Top-of-the-Instrument (TOI)

Charge-changing process happening in materials above L1 are taken into account into the ratio calculation. This determination relies in the MC simulation of materials in front of L1, essentially constituted by supporting structures. In a simple approximation, considering only the background of Carbon going to Boron and indicating with  $\varepsilon_{C \rightarrow B}$  the probability of a charge-changing interaction before L1 then the flux ratio outside from AMS is simply given by  $(B/C)_{\text{TOI}} = (B/C)_{\text{L1}} - \varepsilon_{C \rightarrow B}$ .

Most of the events interacting before L1 are already tagged and rejected by the cuts discussed in section 3.2. The unaccounted effect is small and is translated to an effective correction  $\varepsilon_{C \rightarrow B} = 0.005 \pm 0.002$ .

## 4 Result

The measured Boron-to-Carbon ratio is presented in fig. 6 as a function of the kinetic energy evaluated from the Tracker rigidity. Binning is evaluated according to  $3\sigma$  rigidity resolution of the Tracker. Only events that are traversing AMS from L1 to L8 are used. Events passing through also L9, with lower acceptance but better rigidity resolution, are used for the evaluation of the last bin.

Effect of bin-to-bin event migration due to the finite resolution of the Tracker rigidity has been accounted using an unfolding procedure.

The following sources of systematic error are estimated and included: (a) 2% from MC and data comparison of fragmentation channels; (b) 1% from the error associated to

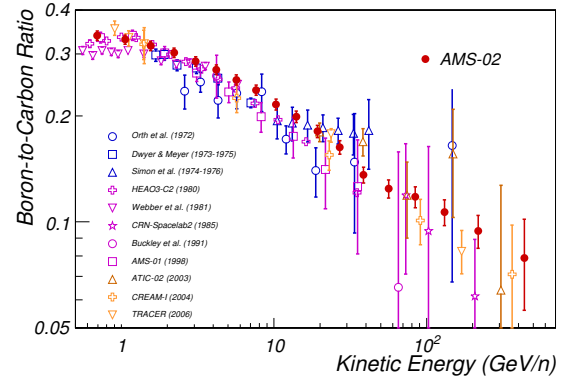


**Fig. 6:** The derived Boron-to-Carbon ratio. Available B/C measurements in the range from 0.5 to 700 GeV/n are shown for comparison: Orth et al. [15], Dwyer and Meyer [16], Simon et al. [17], HEAO3-C2 [18], Webber et al., [19], CRN-Spacelab2 [20], Buckley et al. [21], AMS-01 [22], ATIC-02 [23], CREAM-I [24] and TRACER [25].

the isotopic composition evaluation; (c)  $< 2\%$  from Top-of-the-Instrument correction error; (d)  $< 1\%$  up to 200 GeV/n, and 2% above from the difference between the spectrum and the unfolded spectrum.

## 5 Conclusions

Measurement of the Boron-to-Carbon between 0.5 to 670 GeV/n with AMS-02 has been presented. Main limitation for the ratio measurement and systematics error evaluation at high energy is the statistics. AMS has collected 10% of the expected statistics. The B/C behavior at high energy will become more clear with more data.

**Acknowledgment:** This work has been supported by persons and institutions acknowledged in [10], as well as by the Italian Space Agency under contracts ASI-INFN I/002/13/0 and ASD-C/011/11/1.

## References

- [1] A. Kounine, Int. J. Mod. Phys. E 21, 1230005 (2012).
- [2] S. Haino et al., proceeding to this conference.
- [3] P. Zuccon et al., proceeding to this conference.
- [4] P. Saouter et al., proceeding to this conference.
- [5] Q. Yan et al., proceeding to this conference.
- [6] F. Giovacchini et al., proceeding to this conference.
- [7] W. Sun et al., proceeding to this conference.
- [8] L. Basara et al., proceeding to this conference.
- [9] N. Tomassetti et al., proceeding to this conference.
- [10] M. Aguilar et al., PRL110 141102 (2013).
- [11] M. Aguilar et al., ApJ 736, 105 (2011).
- [12] S. Agostinelli et al., NIM A 506 3 (2003) 250-303.
- [13] J. Ranft, Phys. Rev. D 51, 64 (1995).
- [14] C. Størmer, The Polar Aurora, Oxford, (1950).
- [15] C.D. Orth et al., ApJ 226, 1147 (1978).
- [16] R. Dwyer and P. Meyer, ApJ 322, 981 (1987).
- [17] M. Simon et al., ApJ 239, 712 (1980).
- [18] J.J. Engelmann et al., A&A 233, 96 (1990).
- [19] W. R. Webber et al., proceeding of 19th ICRC (1985).
- [20] D. Muller et al., ApJ 374, 356 (1991).
- [21] J. Buckley et al., ApJ 429, 736 (1994).
- [22] M. Aguilar et al., ApJ 724, 328 (2010).
- [23] A.D. Panov et al., proceeding of 30th ICRC, 3 (2008).
- [24] H.S. Ahn et al., APh 30, 133 (2008).
- [25] A. Obermeier et al., ApJ 752, 69 (2012).